J Mater Sci (2011) 46:7369–7376
DOI 10.1007/s10853-011-5697-z

Microstructure and properties of in situ nanostructured ceramic matrix composite coating prepared by plasma spraying

Xueguang Chen · Yong Yang · Dianran Yan · Yanchun Dong · Lei Wang · Jining He · Jianxin Zhang · Xiangzhi Li

Received: 5 February 2011 / Accepted: 6 June 2011 / Published online: 16 June 2011

Abstract In situ nanostructured ceramic matrix composite coating toughened by metallic phase was fabricated by reactive plasma spraying micro-sized Al–Fe_2O_3 composite powders. The microstructure of the composite coating was characterized by X-ray diffraction, scanning electron microscopy, and transmission electron microscopy, respectively. The adhesive strength, microhardness, toughness, and wear resistance of the composite coating were explored. The results indicated that the composite coating exhibited dense microstructure with a lot of spherical α-Fe and γ-Al_2O_3 nano-sized grains embedded within the equiaxed and columnar $FeAl_2O_4$ nano-grains matrix. The adhesive strength, toughness, and wear resistance of the composite coating were significantly enhanced despite its lower microhardness compared with the micro-sized Al_2O_3 coating, which were attributed to the inclusion of ductile metallic phase Fe in the composite coating and the nanostructure of the composite coating.

Introduction

Surface coating is a unique method to tailor the surface properties of metal component to suit specific environment without sacrificing the bulk characteristics of the metal component [1, 2]. Ceramic coating material is well-known for its superior features, such as high hardness, excellent wear, corrosion, chemical, and thermal resistance [3]. However, its application is limited due to its brittleness and poor machining property. Therefore, many toughening methods have been put forward, in which the inclusion of second phases into ceramic coating material was widely used and investigated [4]. Ceramic matrix composite (CMC) coatings exhibited enhanced toughness and wear resistance compared with monolithic ceramic coatings [5].

In recent years, increasing efforts have been directed toward the synthesis of nanostructured materials because novel and attractive properties can be expected [6, 7]. Nanostructured CMC coatings have been considerably investigated and reported to possess superior adhesion, toughness, spallation, wear, corrosion, and thermal resistance compared to their conventional coarse-grained counterparts [8–10]. A number of techniques have been attempted to produce nanostructured coatings, such as physical vapor deposition, chemical vapor deposition, ion implantation, magnetron sputtering, electrodeposition, laser cladding, thermal spraying, cold spraying, etc. [7, 11–15]. Among the possible processes, reactive plasma spraying (RPS), which combines plasma spraying with self-propagating high-temperature synthesis to produce in situ composite coatings, has received much attention in recent years [16, 17]. The principle of RPS is based on the reaction between feedstock materials or between feedstock materials and surrounding reactive gases present in the plasma. RPS has been used to fabricate thick coatings with improved properties, for example $MoSi_2$/SiC, TiN, Ti–TiN, Fe–TiC, FeCr–TiC, NiCr–TiC, NiCr–Cr_3C_2, etc. [16–23]. However, to the best knowledge of the authors, there is little information about the synthesis of nanostructured CMC coating using RPS.

X. Chen · Y. Yang (✉) · D. Yan · Y. Dong · L. Wang · J. He · J. Zhang · X. Li
Key Laboratory for New Type of Functional Materials in Hebei Province, Hebei University of Technology, Tianjin, China
e-mail: yangyonghebut@163.com; yandianran@126.com

X. Chen · Y. Yang · D. Yan · Y. Dong · L. Wang · J. He · J. Zhang · X. Li
School of Materials Science and Engineering, Hebei University of Technology, No. 29 Guangrong Road, Hongqiao District, Tianjin 300132, China

In this article, we report an efficient method that uses reactive plasma spraying micro-sized Al–Fe_2O_3 composite powders to prepare in situ high-performance nanostructured CMC coating toughened by metallic phase. The microstructure and properties of the as-sprayed nanostructured CMC coating were characterized, and the indentation impression and fracture surface of the CMC coating was carefully analyzed. It is worth noting that the major advantage of this processing route is its simplicity and cost effectiveness which may rapidly lead to mass production and commercial application of nanostructured coating materials.

Materials and methods

Reactive plasma spraying in this investigation is based on the thermite reaction of Al–Fe_2O_3 system. As-received powders are Fe_2O_3 (analytical grade, Tianjin Third Chemical Reagent Co., Ltd., China) with average grain size about 0.6–0.8 μm and Al (99.9% grade, Anshan Iron and Steel Fine Aluminum Powder Co., Ltd., China) with average grain size about 5 μm. The micrographs of the starting powders (Al and Fe_2O_3) were shown in Fig. 1. The Al powders were spherical, and the Fe_2O_3 powders were finely granular. The molar ratio of Fe_2O_3 and Al powders was 1:2. Fe_2O_3 and Al powders were wet-mixed by 99-1A electromotion blender for 12 h using absolute alcohol as the mixing media and polyvinyl alcohol as binder, and then the powder mixture was dried at 150 °C and sieved through the sieve of 200–300 mesh. The carbon steel (0.14–0.22 wt%C) coupons were used as substrates. A bond coating of Ni–10wt%Al self-melting alloy with thickness about 50–100 μm was plasma deposited onto the substrates. The as-prepared Al–Fe_2O_3 composite powders and conventional micro-sized monolithic Al_2O_3 powders (Fig. 2) were then plasma sprayed onto the bond coatings for about 300 μm in thickness, respectively. The plasma spraying parameters were shown in Table 1. The phase constitution of the composite powders and as-prepared coatings was characterized by X-ray diffraction (XRD, Philips X'-Pert MPD) with Cu Kα radiation. A scanning electron microscope (SEM, Philips XL30/TMP) equipped with X-ray energy dispersive spectroscope (EDS) was employed to characterize the morphologies of the composite powders, the cross-sections, fracture surfaces, and indentation impressions of the coatings. The microstructure of the coating was characterized by transmission electron microscope (TEM, Philips Tec-nai F20). The adhesive strength of the coatings (average of three measurements per coating) was measured by tensile adhesion tests according to ASTM C 633-01 [24]. The microhardness was determined on the polished cross-section of the coatings by a HX-1000 Microhardness Tester under an indent load of 100 g with a dwell time of 15 s (ten indents for each sample). Relative toughness of the coatings was expressed by crack extension force (G_c) calculated from Eq. 1 [25]:

$$G_c = 6.115 \times 10^{-4}(a^2 \cdot P/c^3) \quad (1)$$

where G_c is the crack extension force (J m^{-2}), a is the impression half-diagonal (m), P is the indentation load (N), c is the half of the total length (tip-to-tip) of the major crack. Unlubricated sliding wear test was performed on an M-200 tribometer (Xuanhua Material Test Machine Co., Ltd., Xuanhua, China) using block-on-ring configuration in air at room temperature according to ASTM G77-83 [26]. Commercial heat-treated GCr15 steel (0.95–1.05 wt%C, 1.30–1.65 wt%Cr) rings (*HRC* 62) were used to rotate in contact with the coating. The normal load on each block was 500 N. The sliding velocity was about 0.4 m s^{-1}, and the sliding time was 30 min. The wear volume was determined using the wear track data measured by the profile meter, and three specimens were tested for the average value.

Results

Characterization of the composite powders

The XRD pattern of the micro-sized Al–Fe_2O_3 composite powders was shown in Fig. 3a, confirming that the composite powders consisted of Al and Fe_2O_3. Figure 3b

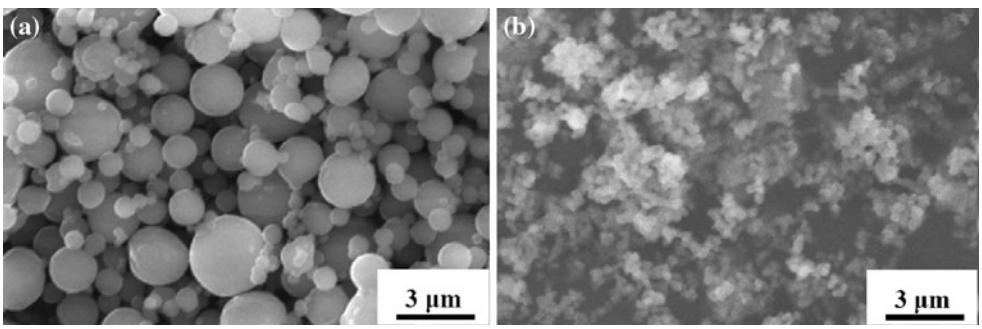

Fig. 1 SEM micrographs of the Al powders (**a**) and Fe_2O_3 powders (**b**)

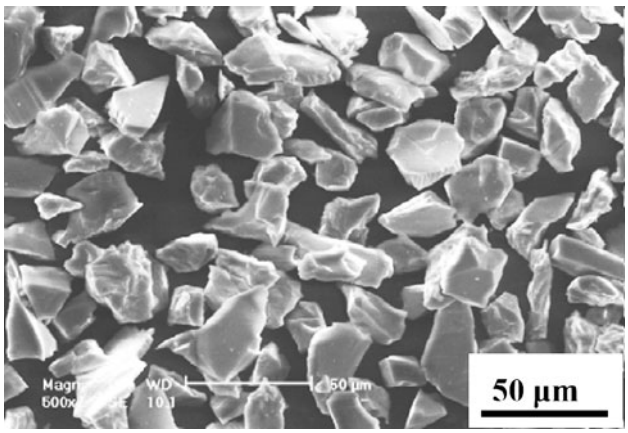

Fig. 2 SEM micrograph of the micro-sized Al_2O_3 powders

showed the SEM micrograph of the composite powders. After reconstitution processing, quasi-spherical composite powders had been obtained. The average particle size of the composite powders was about 50 μm in diameter. Each feedstock particle consisted of many micro-sized Al and Fe_2O_3 granules. Such structure of the composite powders provided homogeneous distribution of Al and Fe_2O_3. Therefore, thermite reaction between Al and Fe_2O_3 may be enhanced to prepare in situ composite with homogeneous composition distribution [27].

Microstructure characterization of the CMC coating

XRD characterization of the CMC coating

The Al–Fe_2O_3 composite powders were then plasma sprayed onto the substrate. Figure 4a showed the XRD pattern of the as-prepared coating, which indicated that the as-prepared coating was mainly composed of $FeAl_2O_4$, γ-Al_2O_3 and α-Fe as a result of the thermite reaction between Al and Fe_2O_3 during plasma spraying. In addition, it can be seen from Fig. 4a that the fundamental diffraction peaks of the CMC coating were fairly broad, indicating that a very fine grain structure was formed in the coating [28].

SEM characterization of the CMC coating

Representative cross-sectional back-scattered SEM micrograph of the CMC coating was shown in Fig. 4b. The cross-sectional view of the CMC coating presented dense and crack-free microstructure with little porosity and good coating-substrate adherence. The porosity of the composite coating was about 3.33 ± 1.02% measured by computerized digital analysis. However, the porosity of the conventional pure Al_2O_3 coating prepared by plasma spraying is generally about 5–10%. The CMC coating exhibited splat morphology (lamellar structure), and the splats were very thin and well-knit. The lamellar splat was derived from melted and spread feedstock powders. The composite powders were better melted during the plasma spraying process due to the high temperature of the plasma jet and the heat released by the reaction of Al–Fe_2O_3 thermite system, which was sufficient to raise the temperature of the feedstock powders to very high value (>3000 K), above the melting points or even the boiling points of reactants, intermediate, and final products [29]. The melted powders, namely the splats, underwent strong spreading and flattening when they impacted on substrate or previously deposited coating due to the high velocity of non-equilibrium plasma spraying process. Hence, the single splat in the CMC coating was very thin and strong adhesion between the splats

Table 1 The main plasma spraying parameters

	Voltage (V)	Current (A)	Primary gas (Ar) flow rate (L min^{-1})	Secondary gas (H_2) flow rate (L min^{-1})	Spray distance (mm)
Ni–Al coating	70	500	80	20	80–100
Al_2O_3 coating	75	500	80	20	80–100
CMC coating	60	500	80	20	80–100

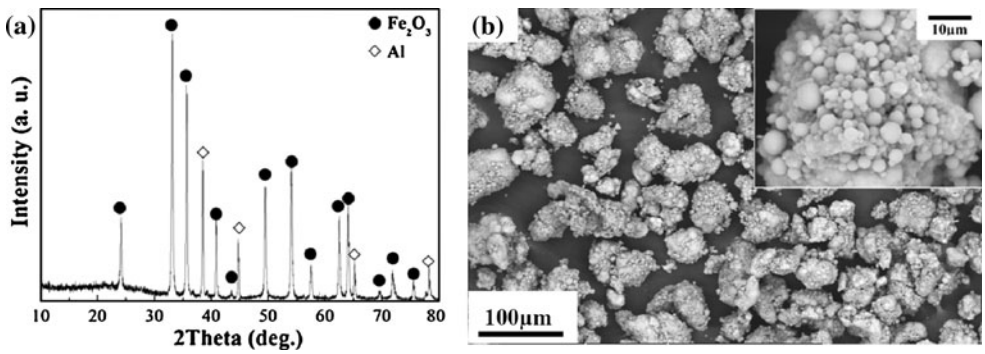

Fig. 3 XRD pattern (**a**) and SEM micrographs (**b**) of the micro-sized Al–Fe_2O_3 composite powders

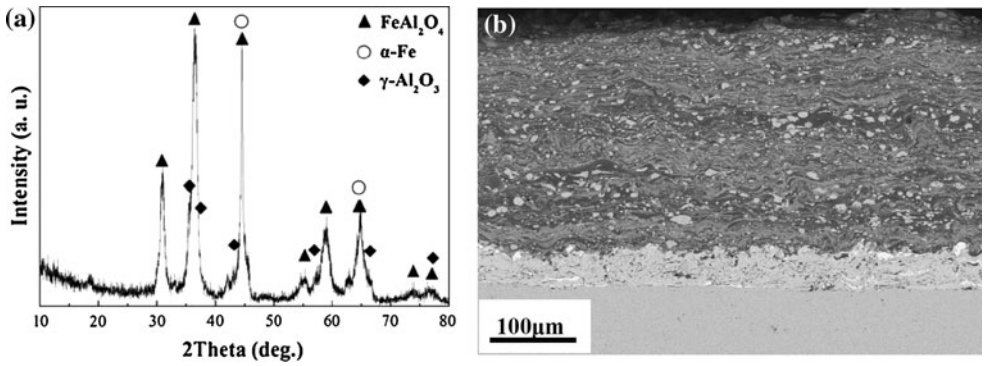

Fig. 4 XRD pattern (**a**) and cross-sectional back-scattered SEM micrograph (**b**) of the CMC coating

was achieved [30]. Some studies revealed that the lamellar bonding (splat adhesion) will determine the properties of plasma sprayed coatings [31].

TEM characterization of the CMC coating

TEM micrographs and the corresponding selected area diffraction (SAD) patterns and EDS results of the CMC coating were shown in Fig. 5. The CMC coating consisted of a large number of fine grains with different morphology, which were on the order of tens of nanometers to hundreds of nanometers. There were equiaxed grains with size about 50–200 nm in the CMC coating (Fig. 5a). The EDS result of "A" area in Fig. 5a (inserted image) exhibited that the equiaxed grains contained Fe, Al, and O, and the SAD pattern (from "A" area in Fig. 5a) of these equiaxed grains

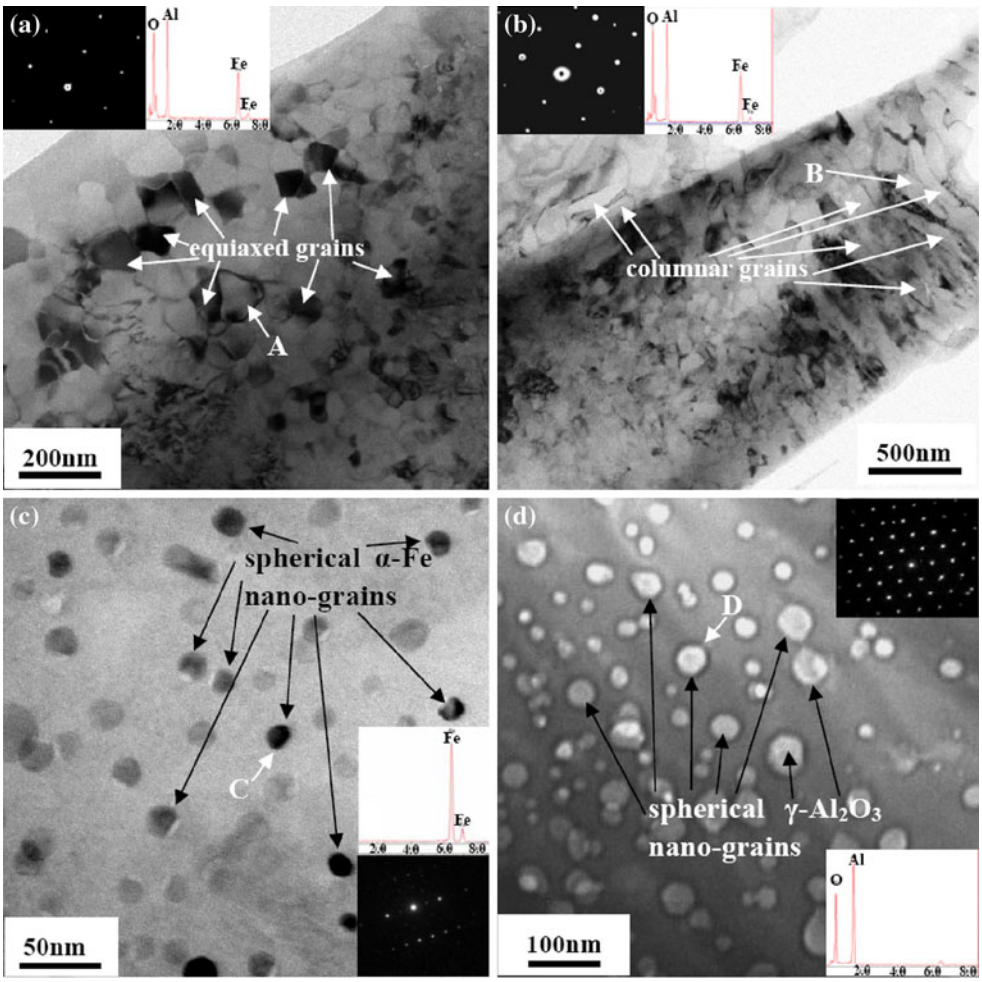

Fig. 5 TEM micrographs and the corresponding SAD patterns and EDS results of the CMC coating: **a** equiaxed $FeAl_2O_4$ nano-grains, **b** equiaxed and columnar $FeAl_2O_4$ nano-grains, **c** spherical α-Fe nano-grains, **d** spherical γ-Al_2O_3 nano-grains

was indexed to $FeAl_2O_4$. Moreover, there were also columnar grains with diameter about 50–100 nm in the CMC coating (Fig. 5b). The EDS result and the SAD pattern (from "B" area in Fig. 5b) of these columnar grains revealed that they were $FeAl_2O_4$. There were a lot of spherical grains with size about 10–200 nm embedded within the matrix (Fig. 5c). The EDS result and the SAD pattern (from "C" area in Fig. 5c) revealed that these spherical grains were α-Fe. There were also a number of spherical grains with size about 10–60 nm embedded within the matrix (Fig. 5d), and the SAD pattern (from "D" area in Fig. 5d) indicated that these spherical grains were γ-Al_2O_3. The TEM characterization results revealed that the CMC coating presented a microstructure with a lot of spherical α-Fe and γ-Al_2O_3 nano-sized grains embedded within the equiaxed and columnar $FeAl_2O_4$ nano-grains matrix. The achievement of dense and crack-free microstructure with metallic phase Fe and ceramic phase Al_2O_3 dispersed homogenously in $FeAl_2O_4$ ceramic matrix will be beneficial to impart the CMC coating high mechanical properties.

Properties of the CMC coating

In order to evaluate the properties of the CMC coating, adhesive strength test, microhardness test, toughness test, wear test, indentation fracture examination, and fractographic study were carried out. Table 2 showed the properties of the CMC coating and conventional micro-sized monolithic Al_2O_3 coating developed using plasma spraying.

Adhesive strength, microhardness, and toughness

The adhesive strength of the CMC coating (26.2 MPa) was higher than that of the Al_2O_3 coating (20.5 MPa). The microhardness of the CMC coating was 900 HV, which was lower than that of the Al_2O_3 coating (1070 HV) due to presence of softer $FeAl_2O_4$ and Fe phases in the coating. However, the crack extension force (G_c) of the CMC coating and the Al_2O_3 coating were 11.3 and 5.4 J m^{-2}, respectively, which indicated that the CMC coating possessed higher toughness (more than double) compared with the Al_2O_3 coating. The toughness-to-hardness (G_c/HV) ratio was considered proportional to the ductility of hard materials [25, 32]. It can be seen (Table 1) that the CMC coating presented higher G_c/HV ratio (1.28) than that of the Al_2O_3 coating (0.51), which suggested a more ductile behavior compared with the Al_2O_3 coating.

Indentation fracture characterization of the CMC coating

Indentation fracture examination was performed on the Al_2O_3 coating and the CMC coating, and the load applied for the Al_2O_3 coating and the CMC coating was 0.98 and 4.9 N, respectively. Figure 6 showed the SEM micrographs of the indentation impressions on the cross-section of the Al_2O_3 coating and the CMC coating. It can be seen that the Al_2O_3 coating was broken along the edge of the indentation impression (Fig. 6a), and multiple cracking (marked by arrows) was present around the indentation impression. However, few microcracks were formed around the

Table 2 Properties of the Al_2O_3 coating and the CMC coating

	Adhesive strength (MPa)	Microhardness (HV)	Microhardness (GPa)	G_c (J m^{-2})	G_c/HV (μm)[a]	Wear volume (mm^3)
Al_2O_3 coating	20.5 ± 2.1	1070 ± 40	10.49 ± 0.39	5.4 ± 1.5	0.51	2.31 ± 0.3
CMC coating	26.2 ± 1.7	900 ± 30	8.82 ± 0.29	11.3 ± 1.8	1.28	0.78 ± 0.1

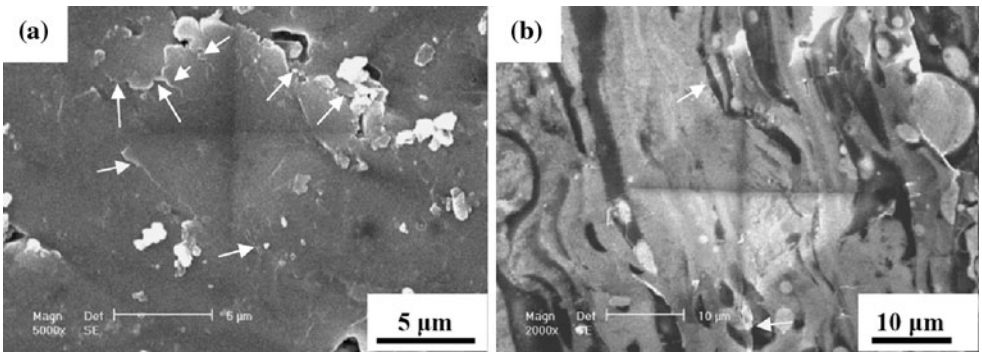

Fig. 6 Indentation impressions on the cross-section of the Al_2O_3 coating and the CMC coating at different loads: **a** the Al_2O_3 coating at load of 0.98 N and **b** the CMC coating at load of 4.9 N

indentation impression on the CMC coating (Fig. 6b). The well-shaped indentation impression and fewer microcracks on the CMC coating, as compared with that on the Al_2O_3 coating, indicated that the CMC coating exhibited a more ductile behavior on indentation than the Al_2O_3 coating. It is known that Al_2O_3 is hard but brittle phase, and stress concentration and fine cracks easily form when the Al_2O_3 coating sustains impact and stress [33, 34]. The presence of tough and ductile Fe phase in the CMC coating can restrain crack propagation by virtue of stress releasing and blunt the cracks. The CMC coating, therefore, showed improved toughness compared with the Al_2O_3 coating. Moreover, the higher toughness of the CMC coating may also be attributed to existence of the nanostructure in the CMC coating.

Fractographic characterization of the CMC coating

The SEM micrographs of the polished cross-sections of the two coatings were shown in Fig. 7. The SEM micrographs of the fracture surfaces of the two coatings were shown in Fig. 8. The Al_2O_3 coating had typical lamellar structure and straight columnar grains (Figs. 7a, 8a). In addition, there were many pre-existing micro cracks and voids between splat boundaries and in the splats of the Al_2O_3 coating. The CMC coating, however, had dense microstructure (Figs. 7b, 8b). The lamellar splats in the CMC coating were thin and well-knit. There were few microcracks in the CMC coating but only some micro spherical pores existed. Previous studies revealed that lamellar microstructure, splat boundaries, pre-existing pores, and cracks usually degraded the performance of plasma sprayed coatings [31, 35]. The achievement of dense and crack-free microstructure would be beneficial to impart the CMC coating high fracture resistance. It can be seen from Fig. 8b that the CMC coating exhibited more ductile mode of fracture compared with the Al_2O_3 coating, which was illustrated by presence of relatively larger number of dimples in the fractograph possibly left by the extracting of the metallic Fe particles.

Wear resistance of the CMC coating

The wear volume of the Al_2O_3 coating and the CMC coating against GCr15 steel was shown in Table 2. The wear volume of the CMC coating was only one-third of that of the Al_2O_3 coating under normal load of 500 N, which meant that the wear resistance of the CMC coating was enhanced by a factor of two compared with the Al_2O_3

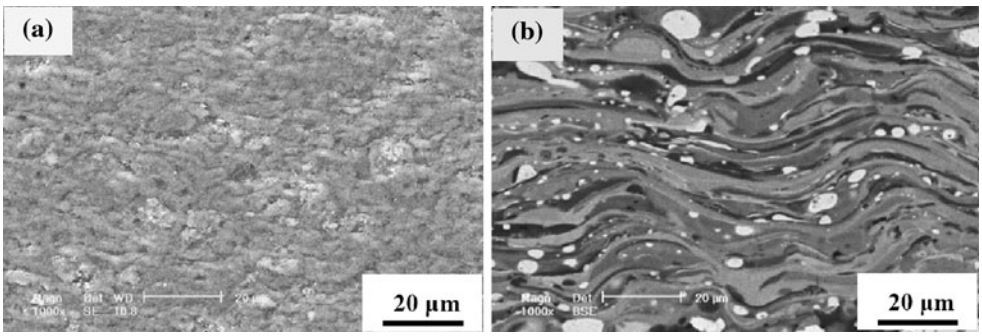

Fig. 7 SEM micrographs of the polished cross-sections of the Al_2O_3 coating (**a**) and the CMC coating (**b**)

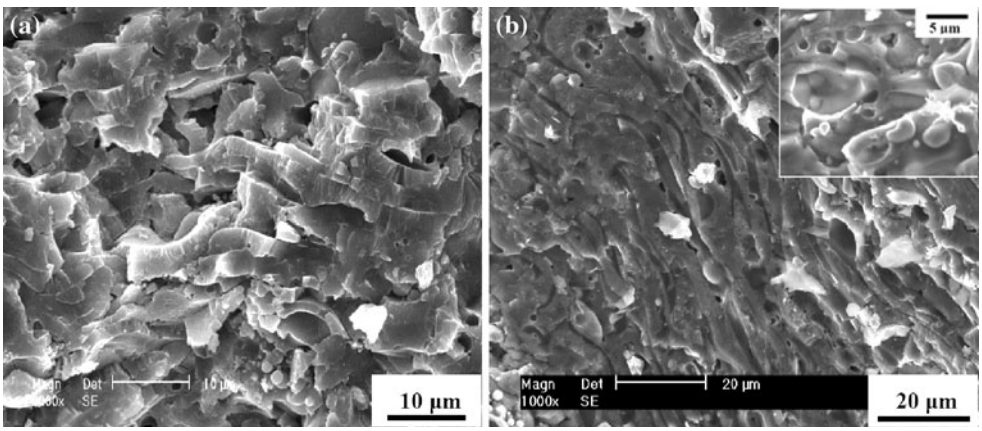

Fig. 8 SEM micrographs of the fracture surfaces of the Al_2O_3 coating (**a**) and the CMC coating (**b**)

coating. The superior wear resistance of the CMC coating to that of the Al_2O_3 coating may be attributed not only to its higher adhesive strength and toughness but also to existence of the nanostructure in the CMC coating [7, 10, 25], which is under further systematic investigation.

Discussion

The molar ratio of Al/Fe_2O_3 in the composite powders was 2:1 in the present investigation, which will lead to reaction products Al_2O_3 and Fe under equilibrium condition according to Eq. 2 [36],

$$2Al + Fe_2O_3 = Al_2O_3 + 2Fe \quad (2)$$

However, it had been pointed out that the chemical composition and phases of the reaction products of Al–Fe_2O_3 thermite system were mainly dependent on the reactants composition, reaction extent, and cooling conditions [29]. It is well-known that the non-equilibrium plasma spraying process is characterized by high temperatures ($\sim$10000 K), high velocity (about 200 m s^{-1}), and extremely high cooling rate (about 10^6–10^8 K s^{-1}) [7, 15, 25]. Therefore, the reaction products ($FeAl_2O_4$, Al_2O_3, and Fe), which were also reported in other non-equilibrium processing of Al–Fe_2O_3 thermite system [29, 37–39], were different from that of the equilibrium reaction condition (Al_2O_3 and Fe). It is known that $FeAl_2O_4$ and Al_2O_3 ceramic phases are hard but brittle, while Fe metallic phase is tough and ductile. Inclusion of metallic phase Fe in $FeAl_2O_4$ ceramic matrix may, therefore, improve the toughness of the ceramic coating effectively.

The micro-sized Al_2O_3 feedstocks were dense and angular. In spray process, the molten state, spread deformation, and adhesion of micro-sized Al_2O_3 feedstocks were not as good as the self-reactive composite powders. Therefore, many microcracks were formed in the Al_2O_3 coating due to the tensile residual stress generated during the rapid cooling process (10^6–10^8 K s^{-1}) and the inhomogeneous solidification of the droplets when spreading out over the substrate [40]. When the load was applied on the Al_2O_3 coating, cracks could be formed and propagate along the pre-existing microcracks as well as lamellar and columnar grain boundaries (GBs). However, the presence of ductile Fe phase in the CMC coating could restrain crack propagation by virtue of stress releasing and blunt the cracks. Therefore, the CMC coating exhibited higher toughness and fracture resistance compared to the Al_2O_3 coating. In addition, as pointed out in [41], grain and interphase boundaries crucially influenced plastic flow and fracture processes in nanocrystalline materials. During plastic deformation, GBs in nanocrystalline materials served as sources of partial lattice dislocations and cracks often nucleated at and grew along interfaces. The nanocrystalline in the CMC coating could play a significant role in improving its fracture and spallation resistance, toughness, and wear resistance.

Conclusion

1) By using reactive plasma spraying Al–Fe_2O_3 composite powders prepared by micro-sized Al and Fe_2O_3 powders, in situ nanostructured ceramic matrix composite coating was synthesized. The composite coating exhibited dense microstructure with a lot of spherical α-Fe and γ-Al_2O_3 nano-sized grains embedded within the equiaxed and columnar $FeAl_2O_4$ nano-grains matrix.
2) The adhesive strength, toughness, and wear resistance of the nanostructured composite coating were significantly enhanced despite its lower microhardness compared with the micro-sized Al_2O_3 coating, which were attributed to the inclusion of ductile metallic phase Fe in the composite coating and the nanostructure of the composite coating.

Acknowledgement The authors gratefully acknowledge the financial supports of the National Natural Science Foundation of China (Grant Nos. 50772028 and 51072045) and the Natural Science Foundation of Hebei province, China (Grant No. E2009000052).

References

1. Padture NP, Gell M, Jordan EH (2002) Science 296:280
2. Donald IW, Mallinson PM, Metcalfe BL, Gerrard LA, Fernie JA (2011) J Mater Sci 46:1975. doi:10.1007/s10853-010-5095-y
3. Gleeson B, Mu N, Hayashi S (2009) J Mater Sci 44:1704. doi:1007/s10853-009-3251-z
4. Becher PF (1991) J Am Ceram Soc 74:255
5. Wang HM, Yu YL, Li SQ (2002) Scr Mater 47:57
6. Xiao L, Yan D, He J, Zhu L, Dong Y, Zhang J, Li X (2007) Appl Surf Sci 253:7535
7. Viswanathan V, Laha T, Balani K, Agarwal A, Seal S (2006) Mater Sci Eng R 54:121
8. Zhou C, Wang N, Wang Z, Gong S, Xu H (2004) Scr Mater 51:945
9. Basak AK, Achanta S, Celis JP, Vardavoulias M, Matteazzi P (2008) Surf Coat Technol 202:2368
10. Bansal P, Padture NP, Vasiliev A (2003) Acta Mater 51:2959
11. Wang W, Hou FY, Wang H, Guo HT (2005) Scr Mater 53:613
12. Pei YT, Shaha KP, Chen CQ, Hulst R, Turkin AA, Vainshtein DI, De Hosson JThM (2009) Acta Mater 57:5156
13. Kim JS, Kwon YS, Lomovsky OI, Dudina DV, Kosarev VF, Klinkov SV, Kwon DH, Smurov I (2007) Compos Sci Technol 67:2292
14. Wang Y, Li CG, Tian W, Yang Y (2009) Appl Surf Sci 255:8603
15. Pawlowski L (2008) Surf Coat Technol 202:4318
16. Liu H, Huang J (2005) J Mater Sci 40:4149. doi:10.1007/s10853-005-2564-9

17. Lavernia EJ, Srivatsan TS (2010) J Mater Sci 45:287. doi: 10.1007/s10853-009-3995-5
18. Mao Z, Ma J, Wang J, Sun B (2009) J Mater Sci 44:3265. doi: 10.1007/s10853-009-3438-3
19. Licheri R, Orru R, Cao G, Crippa A, Scholz R (2003) Ceram Int 29:519
20. Jones M, Horlock AJ, Shipway PH, McCartney DG, Wood JV (2001) Wear 249:246
21. Smith RW, Mutasim ZZ (1992) J Therm Spray Technol 1:57
22. Staia MH, Valente T, Bartuli C, Lewis DB, Constable CP (2001) Surf Coat Technol 146–147:553
23. Deevi SC, Sikka VK, Swindeman CJ, Seals RD (1997) J Mater Sci 32:3315. doi:10.1023/A:1018691826809
24. ASTM C633-01 (2001) In: Annual book of ASTM standard. ASTM, Philadelphia
25. Zois D, Lekatou A, Vardavoulias M (2009) Surf Coat Technol 204:15
26. ASTM G77-83 (1990) In: Annual book of ASTM standards. ASTM, Philadelphia, pp 310–321
27. Yang Y, Wang Y, Tian W, Wang Z, Li C, Zhao Y, Bian H (2009) Scr Mater 60:578
28. Grosdidier T, Tidu A, Liao HL (2001) Scr Mater 44:387
29. Duraes L, Costa BFO, Santos R, Correia A, Campos J, Portugal A (2007) Mater Sci Eng A 465:199
30. Chen H, Zhang YF, Ding CX (2002) Wear 253:885
31. Li CJ, Sun B (2003) Mater Lett 58:179
32. Lawn BR, Marshall DB (1979) J Am Ceram Soc 62:347
33. Hellstern E, Fecht HJ, Garland C, Johnson WL (1989) J Appl Phys 65:305
34. He JH, Schoenung JM (2002) Mater Sci Eng A 336:274
35. Guo HB, Vaßen R, Stover D (2005) Surf Coat Technol 192:48
36. Moore JJ, Feng HJ (1995) Prog Mater Sci 39:275
37. Mei J, Halldearn RD, Xiao P (1999) Scr Mater 41:541
38. Botta PM, Mercader RC, Aglietti EF, Porto Lopez JM (2003) Scr Mater 48:1093
39. Gurt Santanach J, Estournes C, Weibel A, Peigney A, Chevallier G, Laurent Ch (2009) Scr Mater 60:195
40. Westergård R, Axén N, Wiklund U, Hogmark S (2000) Wear 246:12
41. Ovid'ko IA, Sheinerman AG, Aifantis EC (2008) Acta Mater 56:2718